RSC Advances

ROYAL SOCIETY OF CHEMISTRY

www.rsc.org/advances

Role of iron oxidation byproducts in the removal of phosphate from aqueous solution

Nathalie Sleiman[a,b], Véronique Deluchat[a,*], Mahmoud Wazne [c], Alexandra Courtin[a], Zeinab Saad[b], Véronique Kazpard[b], Michel Baudu[a]

[a] Groupement de Recherche Eau Sol Environnement - GRESE EA 4330, University of Limoges, 123 avenue Albert Thomas, Limoges, France

[b] Platform for Research and Analysis in Environmental Sciences, Doctoral School of Science and Technology, Faculty of Sciences, Lebanese University, P.O. Box 5, Campus Rafic Hariri, Hadath, Beirut, Lebanon

[c] Lebanese American University, School of Engineering, Byblos, Lebanon

*Corresponding author at: GRESE EA 4330, University of Limoges, 123 avenue Albert Thomas, Limoges,

France Tel.: +33555457468; Fax+33555457203; E-mail address: **veronique.deluchat@unilim.fr** (V. Deluchat)

Abstract

Zero Valent Iron (ZVI) is widely investigated in water treatment processes, the removal of contaminants may take place at the surface of ZVI or at the surface of its oxidation byproducts flaked off to the bulk solution. In this work, iron byproducts were synthetized under different aeration conditions (4 or 8 mgO_2/L) and aging time (40h or 6 days). The prepared iron oxidation byproducts were characterized using X-ray Diffraction (XRD), Fourier Transform Infrared (FTIR), Raman spectroscopy, Zeta potential, BET surface area, and particle size. XRD analysis showed that the prepared iron oxidation byproducts composed mostly of lepidocrocite, maghemite, and magnetite. These iron oxidation byproducts flaked off were used alone (without ZVI) to remove phosphate. Equilibrium and kinetic studies were conducted to determine the sorption capacities and the rate of phosphate ions uptake at various pH values by the prepared byproducts. The experimental data showed that phosphate sorption adhered to a pseudo second order kinetic model whereas the maximum sorption capacity was determined at 2.5 mgP/g. Phosphate removal capacities of synthetic pure iron oxides and oxy-hydroxides were also determined. Raman and FTIR spectroscopy showed that phosphate was retained by inner sphere complexation.

Key words: Phosphate removal; iron byproducts; adsorption; zero valent iron

1. Introduction

Phosphorus (P) is an essential element needed for plant and biota growth, but excessive amounts of released phosphorus can lead to ecological unbalance manifested by eutrophication, one of the main threats of environmental, sanitary and aesthetic problems in water bodies such as reservoirs and lakes.[1] Phosphorus is released to water bodies from agricultural practices and from the uncontrolled discharge of domestic and industrial wastewater.[1] According to USEPA, to prevent the development of biological nuisances and to control eutrophication, total phosphorus should not exceed 50 µg/L in any stream at the point where it enters any lake or reservoir, or 25 µg/L within the lake or reservoir. A desired goal for the prevention of plant nuisances in streams or other flowing waters not discharging directly to lakes or impoundments is 100 µg/L total P.[2] Moreover, phosphorus concentration in treated wastewater was set by the European Union at 1-2 mg/L according to the directive 91/271/EE.

Various biotic and abiotic factors (pH, ionic strength, water composition, temperature, nature of the adsorbent, …) may affect the speciation, mobility, reactivity and bioavailability of P.[3] However, phosphate can be removed by chemical precipitation, co-precipitation and adsorption by divalent or trivalent metal salts (e.g., aluminum sulfate and ferric chloride).[4,5] Phosphorus can also be removed by biological treatment using microorganisms called *phosphorus accumulating organisms* (PAO) which requires alternating between aerobic and anaerobic conditions.[4] Biological treatment can remove over 85% of phosphorus in wastewater.[6] Recently, the removal of phosphate using adsorption has attracted much attention. Several low cost and waste materials were used for phosphate removal from aqueous solutions using ferric sludge,[7] Al-bentonite, Fe-bentonite and Al-Fe-bentonite,[8] fly ash,[9] alum sludge,[10] iron hydroxide-eggshell waste,[11] magnetic nanocomposites,[12] and Fe(III) modified montmorillonite.[13] Iron oxides and hydroxides are among the low cost materials

used for phosphate removal such as goethite (α-FeOOH),[14,15] akaganeite (β-FeOOH),[14] green rust,[16] and lepidocrocite.[17] Researchers have also investigated the use of iron from iron mine tailing for the sequestration of phosphorus in lake sediments as well as the effects of hypolimnetic aeration on phosphate uptake by iron in lakes.[18,19]

Most recently there has been an increased interest in ZVI for the removal of phosphate from water and wastewater because of its low cost, nontoxic characteristics, good reactivity and potential longevity.[20,21] Phosphate removal by ZVI may take place at the surface of ZVI or at the surface of its byproducts synthesized and flaked off into the bulk solution. The existing data of ZVI efficiency to remove contaminants do not consider separately the reactivity at the surface of ZVI and on the byproducts flaked off from the ZVI surface. In aqueous solutions and under oxic conditions, Fe (0) can be oxidized to Fe (II) which can form ferrous precipitates ($Fe(OH)_2$) at the interface, resulting from the reaction between Fe (II) and OH^- or can be transported away from the surface to form iron byproducts precipitates.[22] The formed ferrous hydroxide will be oxidized to a Fe (II)/Fe (III) mixed phase such as magnetite over time. Maghemite can also be formed on the surface of ZVI.[23,24] Water molecules are the primary oxidant of the Fe (0) surface and Fe (II) is the initial oxidation product. Under anaerobic conditions oxidation of ZVI will be limited due to the lack of oxygen. Furthermore the efficiency of the oxides to remove various species may be affected by aging as reported by Mao et al. (2012) and Smith et al. (2008) who showed that phosphate adsorption onto Hydrous Ferric Oxides (HFO) decreased with the oxide age.[25,26] Oxygen and aging conditions are therefore two main parameters that may highly affect iron byproducts reactivity. Iron fillings are used to remove phosphate but the effects of these two parameters are rarely considered.

In this study only synthesized iron oxidation byproducts (without ZVI) will be used in order to study their efficiencies. The objectives of this study are (i) to determine the composition

and nature of the iron oxidation byproducts prepared under different oxygen and aging conditions, and; (ii) to study the efficiency of the iron oxidation byproducts for phosphate removal at environmental pH.

2. Materials and methods

2.1 Materials

All the chemicals used in this study were of analytical grade. NaCl (99.5 %) was supplied by Fluka, whereas KH_2PO_4 and ZVI (99 %) (Average size about 250 µm) were obtained from Sigma-Aldrich and Jeulin, respectively. Stock solution of 1000 mgP/L was prepared by dissolving an appropriate amount of KH_2PO_4 in ultra-pure water. Adjustment of pH was made with 0.1 M NaOH and 0.1 M HCl.

2.2 Preparation of iron oxidation byproducts

To highlight the role of oxygen in the formation and efficiency of the iron oxidation byproducts, two iron corrosion materials were prepared. The first set was prepared by fixing the aging time at 40 hours and varying the dissolved oxygen concentration between $4mgO_2/L$ (4mg/L-40h) and $8mgO_2/L$ (8mg/L-40h). Similarly, to highlight the role of aging time on the iron oxidation byproducts, two sets of iron oxidation byproducts were prepared , the first set was aged for 40 h (4mg/L-40h) whereas the second set was aged for 6 days (6d-4mg/L).

Oxidation of ZVI was conducted in a 1000 mL beaker at 20±3 ºC by mixing 10 g of ZVI in 1 L of 0.01 M NaCl. For this purpose, a jar test was used at 200 rpm to mix the iron fillings. Oxygen concentration was set at 4 or 8 mg/L in the different reactors. To achieve these oxygen conditions, systems were either pumped with oxygen (using aquarium air pump) or just sealed with parafilm. The concentration of dissolved oxygen in the oxygen saturated systems was kept stable at 8 mg/L for the duration of the experiment; as for the oxygen

limited systems, oxygen concentration dropped from 8 to 4 mg/L during the first hour of the experiment and remained stable at 4 mg/L thereafter.

The pH variation was measured as a function of time using a Mettler Toledo pH-meter whereas dissolved oxygen concentration was measured using an HQ-30d flexi oximeter. Once the iron byproducts were prepared under these different conditions, elemental iron (ZVI) was removed from the suspensions as follow. When the reaction time (40h or 6d) was reached, the beakers were allowed to stand for 30s in order to let the ZVI settle down. The iron oxidation byproducts along with the suspensions, excluding elemental iron (ZVI) settled to the bottom, they were then gently transferred to a new beaker. During this transfer, a magnet was fixed outside, at the bottom of the beaker in order to hinder ZVI transfer. After that, a magnet was dipped in the beaker containing the suspension in order to ensure that no ZVI remained with the suspension. A minor portion of the magnetic iron oxidation byproducts may have been removed by the magnet along with ZVI. In order to compare quantitatively the formation of oxides in the systems with different oxygen concentrations, we defined two fractions namely "particulate" and "filterable". The differentiation between dissolved and particulate iron was based on physical separation by filtration using 0.45 µm syringe filter. Filterable fraction contains both soluble and colloidal iron; however the particulate fraction was obtained by subtracting the filterable fraction from the total iron. Total iron was obtained by acidifying samples for 3 hours at 90 ºC by adding 2 mL of HNO_3 65% and 1 mL HCl 37% for 10 mL of each sample. After acidification, samples were filtered using 0.45µm syringe filter. Samples were then analyzed by flame atomic absorption spectroscopy (AAS) using Varian SpectrAA220; quantification limit was 0.1 mg/L.

The synthesized suspensions (without ZVI) were dried at 40 ºC for 24 hours, then stored in a closed container for later characterization and used for phosphate adsorption.

2.3 Characterization methods

Three samples were characterized to capture the effects of oxygen conditions and aging time on the formation of the iron oxidation byproducts. The set of selected samples included (4mg/L-40h), (8mg/L-40h) and (4mg/L-6d).

These byproducts were identified using XRD, micro-Raman spectroscopy and Fourier Transform – Infrared spectroscopy (FT-IR). In addition, the iron oxidation byproduct samples were characterized before and after phosphate adsorption in order to understand the mechanism of phosphate removal.

XRD patterns for the prepared samples were obtained using a Bruker D8 focus diffractometer using Cu/Kα radiation (λ=0.154 nm). The patterns were then analyzed using X'Pert High Score Plus version 2.0 (by PANalytical B.V.) for peak identification and semi-quantification. The samples were dried and powdered before they were analyzed. Micro-Raman Spectroscopy analyses were performed for structural information using a Horiba Jobin Yvon T 64000. The excitation source was an Ar^+ laser operating at 514.5 nm. The incident power was limited to 2 to 5 mW using density filter to avoid potential deterioration and transformation of the compounds. Typical spectral resolution for the Raman system with an 1800 1/mm grating monochromator was about 2.5 cm^{-1} at the exciting line and the diameter of the laser spot focused on the sample was about 1 μm. FTIR was also used to characterize the functional groups on the surface of the synthesized samples using an FT/IR – 6300 JASCO.

The specific surface area of the iron oxidation byproducts was measured using an ASAP 2020 by Micromeritics whereas the surface morphology was analyzed using a Scanning Electron Microscope (SEM - Philips XL 30, 20 kV). The particle size distribution was obtained by Laser Scattering Particle Size Distribution Analyzer LA950V2 (HORIBA).

Zeta potential was determined by measuring the mobility in an electric field using a Zeta photometer IV Model Z4000. The pH values of the samples were adjusted by using HCl or NaOH to cover the range of pH from 3 to 11. Samples were placed in an electrophoresis chamber and the voltage applied was 95 ± 5 mV. The zeta potential was then calculated automatically by using the Helmholtz-Smoluchowski equation.

The point of zero charge (PZC) was determined by acid base titration of 5 mg/L suspension. Titration was conducted by adding 0.1 M NaOH and HCl every 5 minutes (0.2 mL added every time). Surface charge was calculated according to the equation below:

$$Q= (C_a- C_b + [OH^-] - [H^+]) / m \quad (1)$$

Q is the surface charge in mol/g, C_a and C_b (mol/L) are the concentration of added acid and base respectively and m (g/L) is the solid concentration.

2.4 Synthesis of pure iron oxides and oxy-hydroxides

Lepidocrocite, goethite, maghemite and magnetite were synthesized in the laboratory using the methods of Schwertmann (2000) with minor modifications.[27] Lepidocrocite (Lp) was synthesized by dissolving 11.93 g of $FeCl_2 \cdot 4H_2O$ (60 mmoL Fe) in 300 mL of ultra-pure water with stirring, simultaneously adjusting the pH to 6.7-6.9 with 1M NaOH (120 mL). The suspension was maintained under air flow and stirring for one night. Goethite (Gt) was synthesized by mixing 100 mL of $Fe(NO_3)_3 \cdot 9H_2O$ 1M with 180 mL of NaOH 5 M. Red brown precipitate was formed; the suspension was then diluted to 2 L water and heated at 70 ºC for 60h. Magnetite (Mgt) was synthesized by dissolving 80g of $FeSO_4 \cdot 7H_2O$ in 560 mL deionized water at 90 ºC and by adding 240 mL of free oxygen solution containing 6.46 g of KNO_3 and 44.9 g KOH; the reaction was carried out under N_2 purging. Maghemite (Mgh) was synthesized by heating fresh magnetite in a furnace at 250 ºC for 2 hours. X-ray diffraction data (given in the supplementary information, Fig. S1) revealed that the synthesized solids

were a well-crystallized pure oxides (maghemite and magnetite) and oxy-hydroxides (lepidocrocite and goethite).

2.5 Phosphate sorption experiments

Batch experiments were conducted in 1000 mL closed polyethylene bottles at ambient temperature where the solution volume was set at 200 mL. All experiments were carried out using an orbital agitator (HS 501 Digital IKA-WERKE) at 133 rpm. For the kinetics experiments, adsorbent dose was fixed at 1.5 g/L of iron oxidation byproducts whereas the concentration of phosphate was set at 10 mg/L as P (Ratio Fe/P = 97). The initial pH was set at 7.2 (representative of environmental pH) and remained stable throughout the experiments (pH 7.2 = pKa $H_2PO_4^-/HPO_4^{2-}$). Samples were collected at several time intervals (0, 10', 20', 30', 45', 60', 80', 100', 120', 3 h, 5 h, 8 h, 24 h and 48h). At each sampling time, 1 mL of the homogenized suspension was filtered using 0.45 µm syringe filters and then analyzed for phosphate concentration using a colorimetric method. An antimonyl phosphomolybdate complex was reduced with ascorbic acid, giving blue specie whose absorbance was measured at 880 nm in 1 cm cells with an Agilent 8453 UV-visible spectrometer; the limit of quantification was 100 µg/L.

For the isotherm experiments, the adsorbent dose was fixed at 1.5 g/L and the concentration of phosphate varied from 2 to 20 mg/L as P for the iron byproducts and from 2-100mgP/L for the synthetic oxides and oxy-hydroxides. The pH value and mixing time were respectively fixed to 7.2 and 24 h. This time period of 24h was determined from kinetics experiments as sufficient for reaching equilibrium conditions. Phosphate uptake by the sorbent was calculated as follows:

$$q_t = ([P]_0 - [P]_t) \cdot V / m \quad (2)$$

Where q_t is the adsorption rate (mgP/g adsorbent); $[P]_0$ is the initial concentration of P (mg/L); $[P]_t$ is the concentration of P at time t; V is the volume of the solution (L) and m is the mass of the adsorbent (g).

Pseudo first and second order models were used to simulate the kinetic experiments data whereas Langmuir and Freundlich models were used for the isotherm data results. Equilibrium models can be expressed as follows:

$$q_e = (q_m.K_L.C_e) / (1+K_L.C_e) \quad \text{Langmuir equation,} \qquad (3)$$

$$q_e = K_F C e^n \quad \text{Freundlich equation,} \qquad (4)$$

Where q_e is the amount of phosphate adsorbed onto the solid phase (mgP/g) at equilibrium, q_m is the maximum adsorption capacity (mg/g), C_e is the equilibrium phosphate concentration (mgP/L), K_L is the Langmuir constant (L/mg), K_F ($mg^{n-1/n}$ $L^{1/n}$ g^{-1}) and n are Freundlich constants. The constant n refers to the interaction between surface sites in the adsorbent and phosphate ions in aqueous solution.[14] Non-linear regression analysis was performed using STATISTICA 6.1 for kinetic and isotherm data.

To study the influence of pH on the adsorption of phosphate by the iron byproducts, three different pH values were fixed over time at 4.2, 7.2 and 9.2 for 24 h. The pH was kept stable using an automatic titrator, Titrino 720 with an automatic burette containing HCl 0.1 M or 0.1 M NaOH. Samples were collected as a function of time and filtered at 0.45 µm to be analyzed for phosphate concentration as cited above. The (8mg/L-40h) sample was selected to study of effects of pH on phosphate uptake by iron oxidation byproducts.

3. Results and discussion

3.1 ZVI oxidation monitoring

The variation of pH and the concentration of iron in the dissolved/colloidal fraction (filtrated 0.45 μm) and particulate fraction (total - dissolved/colloidal) were monitored as a function of time. An increase of 1.8 pH unit was observed after about 80 h in the continuous aerated reactor (8 mg/L dissolved O_2) where pH remained constant thereafter (Fig. 1). In the presence of oxygen, oxidation of Fe (0) results in an increase in OH^- concentration which may be responsible for the pH increase (Eqs. (5),(6)). Fe (II) could then be oxidized into Fe (III) releasing more OH^-. As pH increased beyond the onset of precipitation of Fe (II) and Fe (III), both cations fall out of solution as hydroxide precipitates consuming OH^- and thus capping any further increase in pH. When the concentration of dissolved oxygen was limited (4 mg/L), the production of dissolved/colloidal iron and particulate iron was delayed and was lower as compared to the oxygen saturated condition (8 mg/L). The higher pH and particulate Fe concentration in the 8 mgO_2/L system, in comparison with the 4 mgO_2/L system illustrate the role of oxygen concentration in the rates of formation and oxidation of ZVI. Oxygen promoted the corrosion of iron as well as the transformation of Fe (II) to Fe (III) in solutions.[22,28]

The concentration of particulate iron byproducts became significant after 24 hours of reaction and increased over time to attain 3.3 g/L under saturated oxygen conditions after 6 days (results not shown). Equilibrium took place between Fe (II) and OH^- once their rate of production was equal to their rate of consumption through precipitatation.[22,29] Iron oxidation byproducts consisted firstly of a mixture of amorphous and poorly crystallized Fe oxides and the crystallization will increase over time (Eqs. (7) (8)).[30]

$$Fe\ (0) + H_2O + 1/2O_2 \rightarrow Fe\ (II) + 2HO^- \quad (5)$$

$$Fe\ (II) + 1/2H_2O + 1/4O_2 \rightarrow Fe\ (III) + HO^- \quad (6)$$

$$Fe\ (III) + 3H_2O \rightarrow Fe\ (HO)_3 + 3H^+ \quad (7)$$

$$Fe(III) + 2H_2O \rightarrow FeOOH + 3H^+ \quad (8)$$

It is worth noting that the initial colorless solution turned to yellowish in the first minutes for the two oxygen conditions (limited with 4 mg/L and saturated with 8 mg/L). After that, the formed precipitates turned orange then brownish in the 8 mgO_2/L system and black in the limited oxygen condition. Triszcz et al. (2009) suggested that this color change was the result of a shift from particles containing mostly Fe (III) to particles containing Fe (II) and Fe (III) when dissolved oxygen concentration decreased.[22]

3.2 Iron byproducts characterization

XRD patterns (Fig. 2) showed that the prepared iron oxidation byproducts included mostly lepidocrocite and some peaks assigned to maghemite and/or magnetite. Patterns for the different analyzed samples showed peaks at the positions of 14.16º, 27.09º, 36.39º, 38.18º, 46.9º, 52.9º and 60.7º 2θ, which were assigned to lepidocrocite. Lepidocrocite was cited by Huang and Zhang (2005) as the major product of corrosion of ZVI at the initial stages (after 1h) whereas lepidocrocite and magnetite became predominant at later stages.[31] Two peaks observed at 57.4º and 62.6º 2θ were attributed to maghemite and magnetite respectively. Two other peaks observed in all patterns at the positions of 35.5º and 43.3º 2θ may be attributed to maghemite and/or magnetite. All peaks were compared with the XRD database cited by Pecharroman et al. (1995) and Cornell (2003).[32,33] Lepidocrocite, maghemite and/or magnetite were present in the three samples. FTIR spectra (Fig. 3) confirmed the results obtained by XRD. Two strong peaks for lepidocrocite at 742 and 1020 cm^{-1} and a broad shoulder at 1160 cm^{-1} were found in the three different iron byproducts.[33]

Oxygenation between limited and saturated conditions did not seem to have an important effect on the composition of the iron byproducts; the diffractogram of the different samples are very similar indicating the presence of lepidocrocite, maghemite and magnetite (Fig. 2). Likewise, no significant influence of aging was found on the composition of iron byproducts.

The semi-quantitative XRD simulations (given in the supplementary information, Fig. S2) showed the repartition of the different crystallized oxides and oxy-hydroxides in the iron oxidation byproducts samples.

SEM images (Fig. 4) showed a homogeneous morphology for the different samples (4mg-40h, 8mg-40h, 4mg-6d) where some crystals characteristic of lepidocrocite with short lath like shape were observed with a size approximately about 3 to 6 µm in length..

Table 1 shows the average surface area and particle size for the three samples. Particle size was similar for the different conditions, about 6 µm. After 40 h in the two oxygen conditions, the specific surface areas were very close between 63 and 69 m^2/g. However upon further aging from 40 h to 6 days, the samples exhibited lower surface area measured at 46 m^2/g. Surface areas were found not correlated with the diameter of the particles and thus indicated differences in the structure of aggregates.

Table 1: Average diameter (µm) and surface area (m^2/g) of the oxy-hydroxides synthesized in three different conditions.

Samples	4mg/L- 40h	8mg/L- 40h	4mg/L-6d
Particle size (µm)	5.9±0.8	6±2	6.1±0.3
Surface area (m^2/g)	63±1	69±1	46±1

One of the most important parameters in adsorption studies is the surface charge of the adsorbent because it serves as an indicator of reactivity and stability of the material. It influences the affinity between anions and cations, stability and particle interactions.[34] For this purpose, Point of Zero Charge (PZC) and IsoElectric Point (IEP) measurements were conducted for the three different iron byproducts (Table 2). Table 2 shows no significant variation in IEP and PZC with the age of oxy-hydroxides (40 h and 6 days). However, oxygen concentration showed limited influence on the surface charge; IEP and PZC increased when

oxygen concentration increased for the 40 h samples. In theory, when there is no specific adsorption, IEP and PZC should be equal. In our case there was a small offset between PZC and IEP which could be due to the fixation of impurities on the surface of the material.

Table 2: PZC and IEP measurements for the different oxy-hydroxides.

Samples	4mg/L-40h	8mg/L-40h	4mg/L-6d
PZC	6.0±0.2	7.0±0.2	6.3±0.1
IEP	6.9±0.1	7.4±0.1	6.8±0.1

In order to understand the mechanism of phosphate removal using these byproducts, a comparison of the spectra before and after phosphate adsorption was conducted. As the samples did not show significant differences in their composition and reactivity, only one sample was analyzed. FTIR and RAMAN spectroscopy analysis were compared for the sample 8mg/L-40h before and after phosphate adsorption. A comparison of the FTIR and Raman spectra was also conducted for the unloaded and phosphate loaded byproducts in order to determine any new peaks, intensity variation or wavelength shifts (Fig. 3 and 4). The FTIR spectra showed a strong and broad band between 3000 and 3600 cm^{-1} which was associated with the O-H stretching vibrations of the hydroxyl groups in the layers and interlayers water molecules (Fig. 3).[35] Another absorption band corresponding to water with O-H bending vibrations was recorded around 1634 cm^{-1} indicating physisorbed water molecule on the surface of the adsorbent. Strong peaks at 742 and 1020 cm^{-1} confirmed the presence of surface hydroxyls of lepidocrocite.[33] After phosphate adsorption, a new peak appeared at 890 cm^{-1} and 1077 cm^{-1} which were broad; these peaks could be assigned to the vibration of P-OH and the asymmetry vibration of P-O bond, respectively, indicating that the surface hydroxyl groups could be replaced by the adsorbed phosphate (Fig. 3). It may be deduced that the surface hydroxyl groups (M-OH) could be exchanged with phosphate (M-O-P) which

possibly indicates the formation of inner-sphere surface complex between phosphate and these iron byproducts.[36,37]

Raman spectra of the synthesized byproduct in 8mg/L-40h before and after phosphate adsorption are displayed in Fig.4. Before adsorption, two sharp peaks at 250 and 373 cm^{-1} and three broad peaks at 520, 651, and 1295 cm^{-1} were ascribed to lepidocrocite according to the Raman spectrum of synthetic lepidocrocite.[33,38,39] After adsorption of phosphate (10 mgP/L), new peaks were identified in the Raman spectrum. Strong peaks were identified at 215 and 300 cm^{-1} and can be attributed respectively to lepidocrocite and goethite. The vibration bands of the anions intercalated in the interlayers of the iron oxides were very weak. Two new broad peaks appeared after phosphate adsorption at 1050 and 1135 cm^{-1} and could be assigned to the stretching vibration band of P-O.[40,41] Raman and FTIR results indicated the replacement of the hydroxyl groups by phosphate which confirmed the formation of inner sphere complex.

3.3 Phosphate removal

3.3.1 Kinetics and isotherms experiments

Several factors can influence phosphorus retention capacities and adsorption kinetics such as surface area, crystallinity and morphology of the iron oxides. Experiments were conducted to investigate the kinetics of phosphate removal from water using the different iron byproducts.

The adsorption constant values for the pseudo second order model, the correlation coefficients R^2, and the predicted q_e values are given in Table 3. Based on values of the correlation coefficient (R^2) of the iron oxidation byproducts, pseudo second order model ($R^2 \geq 0.96$) was found to better fit than the pseudo first order one ($R^2 \leq 0.92$), thus the data of the pseudo first order will not be shown here. Pseudo second order model indicates that adsorbent interacts with two surface sites.[16] The samples aged for 40 h (both 4mg/L O_2 and 8mg/L O_2), showed

the same uptake capacity near 2.4 mg/g iron oxidation byproducts where no influence of oxygen was found for these different conditions. Phosphate removal percentages were 23, 37 and 39% for the samples 4mg/L-6d, 8mg/L-40h and 4mg/L-40h, respectively.

Table 3: Pseudo second order Kinetic parameters for the sorption of phosphate onto the synthesized oxy-hydroxides (40h-4mg/L, 40h-8mg/L, 6d-4mg/L) and the synthetic goethite, lepidocrocite, maghemite and magnetite. Adsorbent concentration = 1.5 g/L; [P] = 10 mg/L, T=20 °C, NaCl = 0.01 M.

Samples	K ($g.mg^{-1}.min^{-1}$)	q_e (mg/g)	R^2
4mg/L-40h	2.3±0.6	2.20±0.07	0.97
8mg/L-40h	2.5±0.6	2.00±0.07	0.96
4mg/L-6d	4±2	1.40±0.05	0.96
Goethite	2.8±0.6	1.40±0.04	0.98
Lepidocrocite	9±2	2.03±0.05	0.98
Maghemite	6±2	0.56±0.02	0.97
Magnetite	8±6	0.40±0.03	0.90

Figure 6 represents the isotherms (experimental data, Langmuir and Freundlich models). Isotherm results for the iron oxidation byproducts indicated that Freundlich model was a better fit for the experimental data, in accordance with the observations of Chitrakar et al.(2006) (Table 4 and Fig.6).[14] It appears that there is a progressive saturation during adsorption with modification of the surface properties. The adsorption capacities of the adsorbents synthesized after 40 h in two different oxygen conditions were similar, q_m= 2.5±0.1 mgP/g iron oxidation byproduct (3.8 mgP/gFe) and 2.42±0.09 mgP/g ron oxidation byproduct (3.7 mgP/gFe) for 4mg/L-40h and 8mg/L-40h respectively. The sample prepared using 6 days under oxygen limited conditions showed the lowest adsorption capacity (q_m = 1.5±0.1 mgP/g iron oxidation byproduct; 2.3mgP/gFe). The difference in the phosphate uptake between samples aged for 40 h and 6 days can be attributed to aging effect; as aging time increased, the efficiency decreased. An increase in the crystallinity over time can take place and amorphous iron oxides can be transformed to crystalline phases. This mineral

transformation could explain the decrease of the surface area and the subsequent decrease of phosphate sorption.[42] These results are in agreement with previous aging effect work published in the literature

Table 4: Freundlich and Langmuir models regression constants for phosphate removal by the three different iron byproducts and synthesized iron oxides. Adsorbent concentration = 1.5 g/L; [P] =2-20 mg/L (iron byproducts) and 2-100 mg/L (iron oxides and oxy-hydroxides), T=20 °C, NaCl = 0.01 M.

	Langmuir constants			Freundlich constants		
	q_m (mg/g)	K_L (L/mg)	R^2	K_F ($mg^{n-1/n} L^{1/n} g^{-1}$)	n	R^2
4mg/L-40h	2.5±0.1	22±8	0.98	1.93±0.05	0.12±0.02	0.99
8mg/L-40h	2.42±0.09	10±4	0.97	1.78±0.06	0.14±0.01	0.98
4mg/L-6d	1.5±0.1	4.±2	0.92	1.2±0.2	0.1±0.06	0.92
Goethite	2.16±0.09	1.9±0.7	0.98	1.5±0.3	0.1±0.05	0.95
Lepidocrocite	3.2±0.2	4±2	0.98	2.0±0.2	0.13±0.02	0.99
Maghemite	1.0±0.1	0.5±0.4	0.90	0.5±0.1	0.16±0.08	0.90
Magnetite	0.68±0.04	0.5±0.2	0.97	0.39±0.09	0.13±0.07	0.92

Mao et al. (2012) showed that the more the hydrous ferric oxides are aged, the lower the phosphate removal is, without any information given about the physico-chemical characteristics of the samples.[25] The apparent capacity of phosphate removal determined by Berkowitz et al. (2006) using aluminum hydroxides ($Al(OH)_3$) decreased also with aging of the hydroxides (from 4 to 180 days of aging); as floc age increased, the crystallinity increased too, which was responsible for the decreased adsorption capacities over time. [42]

Direct comparison with previous work was difficult as no published data were found on phosphate sorption using only iron byproducts without ZVI.

Table 5: Phosphate adsorption capacities of common iron oxides and oxy-hydroxides.

Sorbent	pH	Capacity mgP/g	[adsorbent] g/L	[P] mg/L	Ref.
Magnetite	3.0	5.2	1	n.d.	[43]
Magnetite	7.2	0.68	1.5	2-100	This study
Goethite	7.2	2.16	1.5	2-100	This study
Goethite	2.0	25	1	50	[14]
Goethite	7.0	18	1	50	[14]
Goethite	10.7	6	1	50	[14]
Goethite	7.0	6.3	2	0-50	[44]
Goethite	3.9	2.48	1	1.25-13.75	[45]
Goethite	9.0	1.75	1	1.25-13.75	[45]
Lepidocrocite	5.0	8.2	2	3.1-93	[17]
Lepidocrocite	7.2	3.17	1.5	2-100	This study
Maghemite	7.2	0.98	1.5	2-100	This study
Iron byproducts (4mg/L-40h)	7.2	2.5	1.5	2-20	This study

It appears that few data are available in the literature on phosphate removal using different oxides or oxy-hydroxides at encountered environmental conditions. Experimental conditions were mostly pertaining to acidic pH conditions. Therefore, phosphate sorption capacities of synthetic iron oxides were investigated. The four iron oxides (maghemite, magnetite) and oxy-hydroxides (lepidocrocite, goethite) identified as iron oxidation byproducts in our experimental conditions, were studied. Results of adsorption isotherms by the prepared synthetic oxides and oxy-hydroxides under similar experimental conditions showed maximum removal capacities of 3.17 mg/g, 2.16 mg/g, 0.98 mg/g, and 0.68 mg/g for lepidocrocite, goethite, maghemite, and magnetite, respectively. Direct comparison between the phosphate sorption capacities obtained with synthetic iron oxides and the iron oxidation byproducts cannot be done, as many parameters can influence their capacities such as surface area, PZC… However as iron byproducts contain these iron oxides and oxy-hydroxides, it is

interesting to underline that low range phosphate sorption capacities were obtained for all these supports. By comparing phosphate sorption capacities obtained in this work with the uptake capacities of other adsorbents for phosphate removal reported in the literature, it appears that the capacities of the iron byproducts obtained in this work were mostly lower (Table 5). However, in same experimental conditions, the highest sorption capacities reported in the literature were for experiments conducted with low pH conditions (3 or 5), which favor anionic species sorption and are not representative of environmental conditions.

3.3.2 Effect of pH

Figure 6 shows that the adsorption capacity decreases from 3.77 to 1.44 mg/g with pH increasing from 4.2 to 9.2 respectively, with 8mg/L-40h. When pH increased, the surface charge of synthesized iron byproducts varied from positive to negative, according to the point of zero charge (between 6.0 and 7.0) due to deprotonation of surface hydroxyls. At the same time, the phosphate species exist in solution in different forms ($H_2PO_4^-$ and HPO_4^{2-}) and at different ratios depending on pH. The three pKa of phosphate species are pKa_1 ($H_3PO_4/H_2PO_4^-$) = 2.2, pKa_2 ($H_2PO_4^-/HPO_4^{2-}$) = 7.2 and pKa_3 (HPO_4^{2-}/PO_4^{3-}) = 12.2. Phosphate anions change from mono- to dibasic, then an electrostatic repulsion with the oxides takes place.[43] The phosphate uptakes by common oxides are summarized in Table 5. It can be observed that the highest adsorption capacities for the various adsorbents in the same experimental conditions are found to pH close to 4, which is in agreement with our results. Thus it indicates that iron oxides have more affinity for the monovalent form of phosphate ($H_2PO_4^-$). As pH increases, adsorption decreases due to the competition between OH^- and phosphate anions.[14,16] Beyond the IEP value, a negatively charged oxides lead to lower phosphate adsorption.[8] In our study we fixed the pH at 7.2 during the kinetics and isotherms experiments to represent water treatment conditions; however this pH is not the optimal one

for the highest phosphate adsorption efficiency. To further investigate the uptake of phosphate at neutral pH it is worthwhile looking at the speciation of phosphate as a function of pH and at the PZC values of the iron byproducts.[46] The PZC of the iron byproducts were found to range between 6.0 and 7.0 (Table 2). Phosphate adsorption onto iron oxides has been widely investigated and the main mechanisms are reported based on specific and nonspecific adsorption: ligand exchange and electrostatic interaction. The electrostatic bonding is based on the charge of the surface and the charge of the sorbed ions. Electrostatic based removal predominates when the oxide surface has positive global charge and phosphate species is negatively charged.[9] In our case, as the surface charge of the byproducts is zero or negative, there will be no adsorption of anions through electrostatic adsorption. In contrast where specific adsorption is involved, an overall positive surface charge is not required, which explains why adsorption can occur at pH above the PZC.[5]

4. Conclusion

Synthesized iron oxidation byproducts in the three different conditions (4 or 8mgO_2/L, aging time 40h or 6 days) were mainly formed by lepidocrocite with presence of some peaks of maghemite and magnetite. The kinetic data were better described by a pseudo second order adsorption kinetic model. The maximum sorption capacity was determined at 2.5 mg/g for the 4mg/L-40h sample. This result was in the same range as phosphate sorption capacities obtained with pure lepidocrocite, maghemite and magnetite. FTIR and Raman results indicated an exchange of the hydroxyl group by phosphate via the formation of inner sphere complex was the main mechanism responsible for phosphate adsorption on the surface of the iron byproducts. The operating conditions (pH, dissolved oxygen concentrations and aging) strongly affect the nature of the oxidation of iron fillings and therefore the sorption properties

of the byproducts. These operating conditions need to be framed in a very precise model in order to implement applicable reaction pathways using this support material.

Acknowledgments

This research has been financed by research grant programs of the Lebanese University. Funding was also provided by University of Limoges. We acknowledge the support of AZM and SAADE association, PCSI programs in AUF and PHC Cèdre (PHOSFER project).

References

1 F. Khan and A. Ansari, *Bot. Rev*, 2005, **71**, 449–482.
2 K. M. Mackenthun, *Toward a Cleaner Aquatic Environment*, Environmental Protection Agency, Office of Air and Water Programs, U.S., 1973.
3 Y. Arai and D. L. Sparks, *J. Colloid Interface Sci.*, 2001, **241**, 317–326.
4 G. Morse, S. Brett, J. Guy and J. Lester, *Sci. Total Environ.*, 1998, **212**, 69–81.
5 E. N. Peleka and E. A. Deliyanni, *Desalination*, 2009, **245**, 357–371.
6 S. K. Ramasahayam, L. Guzman, G. Gunawan and T. Viswanathan, *J. Macromol. Sci. Part A*, 2014, **51**, 538–545.
7 X. Song, Y. Pan, Q. Wu, Z. Cheng and W. Ma, *Desalination*, 2011, **280**, 384–390.
8 L. Yan, Y. Xu, H. Yu, X. Xin, Q. Wei and B. Du, *J. Hazard. Mater.*, 2010, **179**, 244–250.
9 J. Chen, H. Kong, D. Wu, X. Chen, D. Zhang and Z. Sun, *J. Hazard. Mater.*, 2007, **139**, 293–300.
10 A. O. Babatunde and Y. Q. Zhao, *J. Hazard. Mater.*, 2010, **184**, 746–752.
11 N. Y. Mezenner and A. Bensmaili, *Chem. Eng. J.*, 2009, **147**, 87–96.
12 S. K. Ramasahayam, G. Gunawan, C. Finlay and T. Viswanathan, *Water. Air. Soil Pollut.*, 2012, **223**, 4853–4863.
13 L. Borgnino, C. E. Giacomelli, M. J. Avena and C. P. De Pauli, *Colloids Surf. Physicochem. Eng. Asp.*, 2010, **353**, 238–244.
14 R. Chitrakar, S. Tezuka, A. Sonoda, K. Sakane, K. Ooi and T. Hirotsu, *J. Colloid Interface Sci.*, 2006, **298**, 602–608.
15 C. Luengo, M. Brigante and M. Avena, *J. Colloid Interface Sci.*, 2007, **311**, 354–360.
16 K. Barthélémy, S. Naille, C. Despas, C. Ruby and M. Mallet, *J. Colloid Interface Sci.*, 2012, **384**, 121–127.
17 J. Kim, W. Li, B. L. Philips and C. P. Grey, *Energy Environ. Sci.*, 2011, **4**, 4298–4305.
18 M. Clayton, S. Liegeois and E. Brown, *Soil Sediment Contam.*, 2004, **13**, 421–431.
19 D. J. McQueen, D. R. S. Lean and M. N. Charlton, *Wat. Res*, 1986, **20**, 1129–1135.
20 Z. Wen, Y. Zhang and C. Dai, *Colloids Surf. Physicochem. Eng. Asp.*, 2014, **457**, 433–440.
21 T. Almeelbi and A. Bezbaruah, *J. Nanoparticle Res.*, 2012, **14**, 900–914.
22 J. M. Triszcz, A. Porta and F. S. G. Einschlag, *Chem. Eng. J.*, 2009, **150**, 431–439.

23 J. Farrell, J. Wang, P. O'Day and M. Conklin, *Environ. Sci. Technol.*, 2001, **35**, 2026–2032.
24 K. K. Mar, D. Karnawati, Sarto, D. P. E. Putra, T. Igarashi and C. B. Tabelin, *Procedia Earth Planet. Sci.*, 2013, **6**, 242–250.
25 Y. Mao, A. Ninh Pham, Y. Xin and T. David Waite, *Sep. Purif. Technol.*, 2012, **91**, 38–45.
26 S. Smith, I. Takacs, S. Murthy, G. T. Daigger and A. Szabo, *Water Enviroment Res.*, 2008, **80**, 428–438.
27 U. Schwertmann, *Iron oxides in the laboratory: preparation and characterization*, Wiley-VCH, Weinheim ; New York, 2nd completely rev. and extended ed., 2000.
28 H. Liu, T. Chen, X. Zou, Q. Xie, C. Qing, D. Chen and R. L. Frost, *Chem. Eng. J.*, 2013, **234**, 80–87.
29 N. El Azher, B. Gourich, C. Vial, M. B. Soulami and M. Ziyad, *Chem. Eng. Process. Process Intensif.*, 2008, **47**, 1877–1886.
30 M. Komárek, A. Vaněk and V. Ettler, *Environ. Pollut.*, 2013, **172**, 9–22.
31 Y. H. Huang and T. C. Zhang, *Water Res.*, 2005, **39**, 1751–1760.
32 C. Pecharroman, T. Gonzalez-Carreno and J. Iglesias, *Phys. Chem. Miner.*, 1995, **22**, 21–29.
33 R. M. Cornell, *The iron oxides: structure, properties, reactions, occurrences, and uses*, Wiley-VCH, Weinheim, 2nd, completely rev. and extended ed., 2003.
34 Y. Ji, *Colloids Surf. Physicochem. Eng. Asp.*, 2014, **444**, 1–8.
35 H. Liu, X. Sun, C. Yin and C. Hu, *J. Hazard. Mater.*, 2008, **151**, 616–622.
36 P. Persson, N. Nilsson and S. Sjöberg, *J. Colloid Interface Sci.*, 1996, **177**, 263–275.
37 G. Zhang, H. Liu, R. Liu and J. Qu, *J. Colloid Interface Sci.*, 2009, **335**, 168–174.
38 P. Refait, M. Reffass, J. Landoulsi, R. Sabot and M. Jeannin, *Colloids Surf. Physicochem. Eng. Asp.*, 2007, **299**, 29–37.
39 D. L. A. De Faria, S. Venaü ncio Silva and M. T. de Oliveira, *J. Raman Spectrosc.*, 1997, **28**, 873–878.
40 M. Bouchard and D. C. Smith, *Spectrochim. Acta. A. Mol. Biomol. Spectrosc.*, 2003, **59**, 2247–2266.
41 Y. Lai, X. Liang, S. Yang, P. Liu, Y. Zeng and C. Hu, *J. Alloys Compd.*, 2014, **617**, 597–601.
42 J. Berkowitz, M. A. Anderson and C. Amrhein, *Water Res.*, 2006, **40**, 911–916.
43 T. J. Daou, S. Begin-Colin, J. M. Grenèche, F. Thomas, A. Derory, P. Bernhardt, P. Legaré and G. Pourroy, *Chem. Mater.*, 2007, **19**, 4494–4505.
44 O. K. Borggaard, B. Raben-Lange, A. L. Gimsing and B. W. Strobel, *Geoderma*, 2005, **127**, 270–279.
45 Z. Ioannou, A. Dimirkou and A. Ioannou, *Water. Air. Soil Pollut.*, 2013, **224**,1374–1388.
46 P. Hinsinger, *Plant Soil*, 2001, **237**, 173–195.

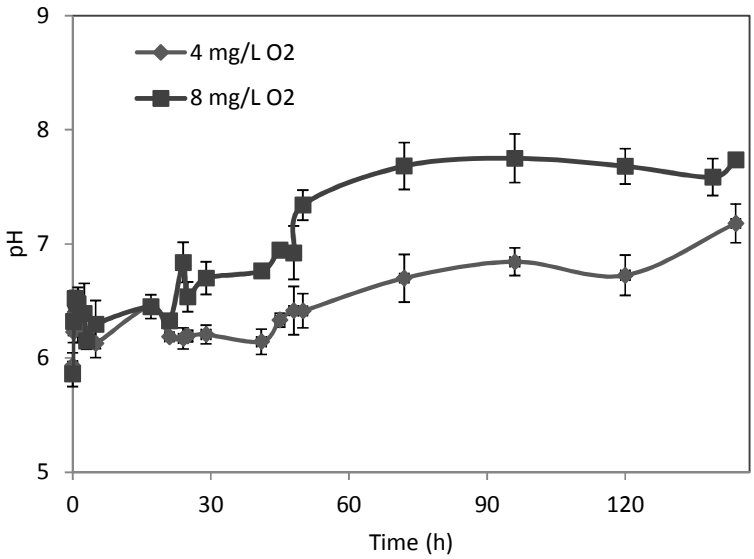

Fig. 1 pH evolution as a function of time in the working suspensions. Conditions: 10 g/L of ZVI, NaCl 0.01 mol/L, in two different oxygen condition (4 and 8mg/L), at T = 20°C.

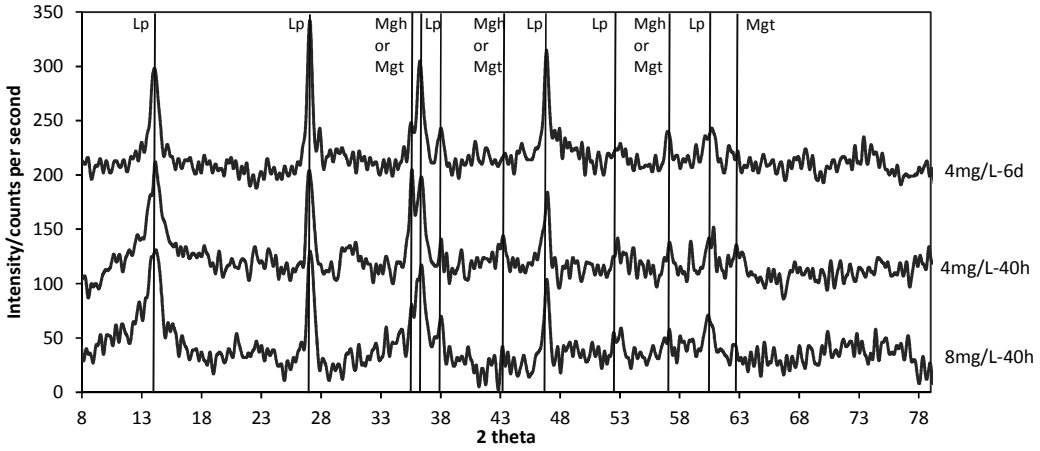

Fig. 2 XRD patterns of the different synthesized iron oxidation byproducts (8mg/L-40h, 4mg/L-40h, 4mg/L-6d). Legend: Lp for lepidocrocite, Mgh for maghemite and Mgt for magnetite.

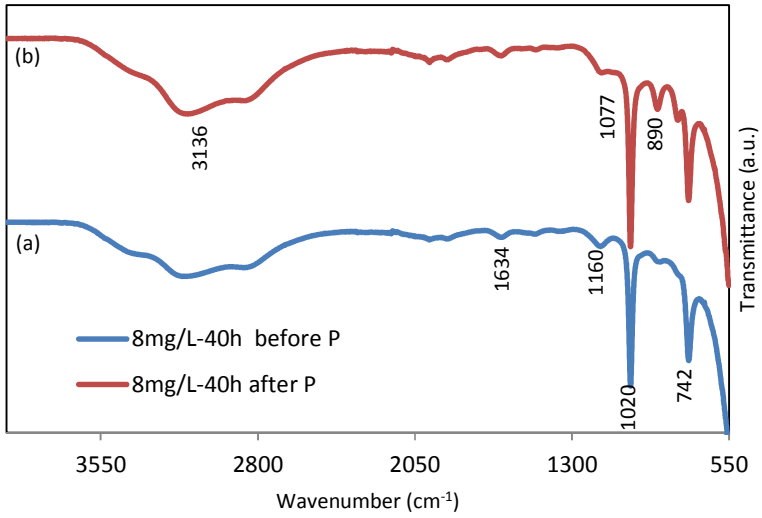

Fig. 3 FTIR spectra of the 8mg/L-40h sample before (a) and after phosphate adsorption (40mgP/L) (b).

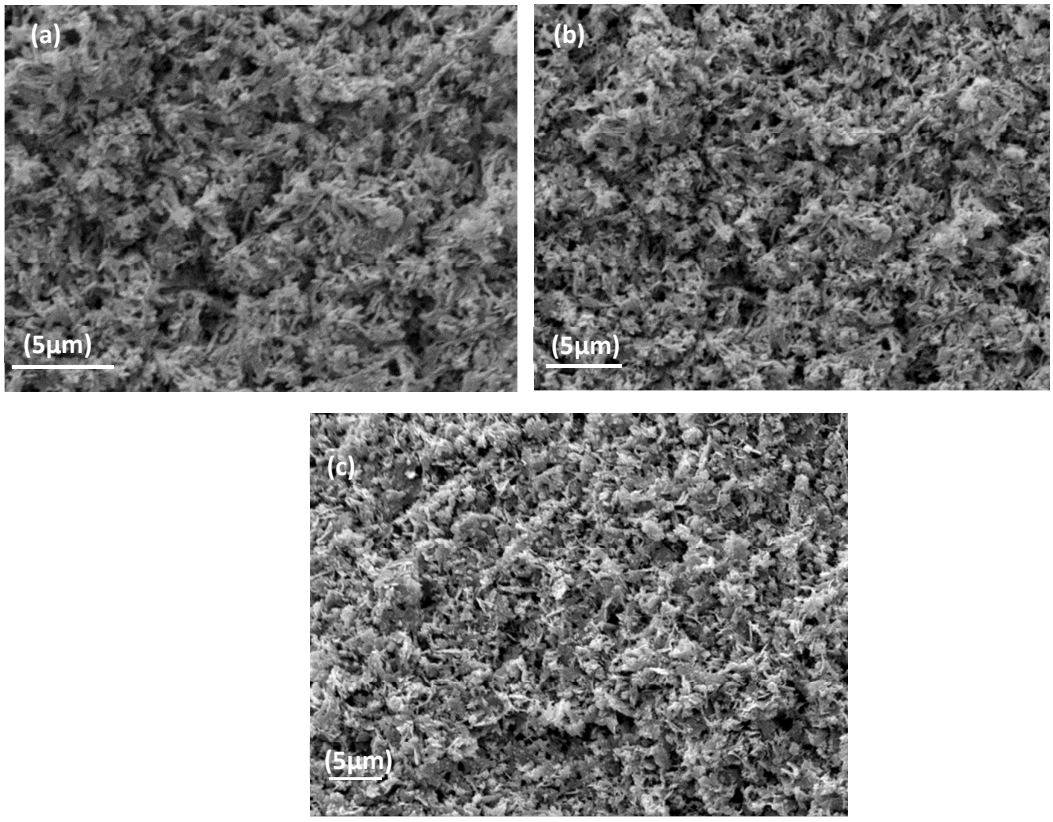

Fig. 4 SEM images for the samples (a) 8mg/L-40h, (b) 4mg/L-40h and (c) 4mg/L-6d.

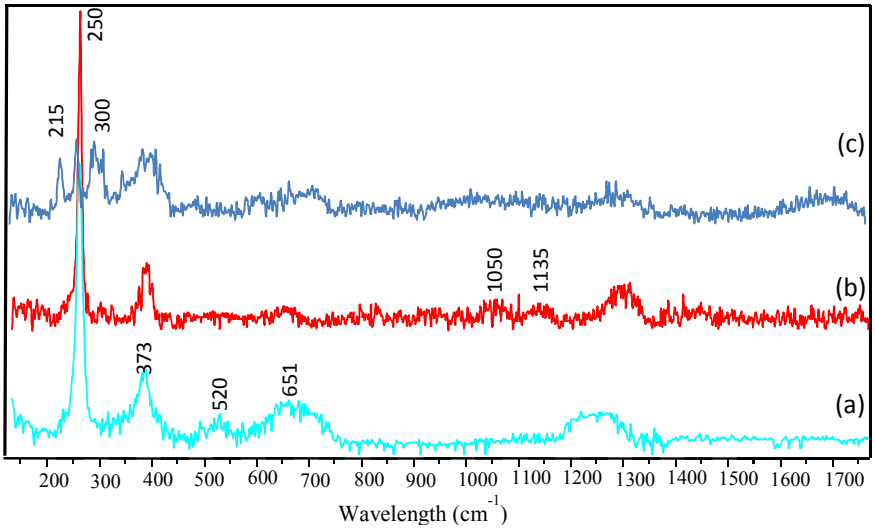

Fig. 5 Raman spectra of the iron oxidation byproducts (8mg/L-40h) before (a) and after phosphate adsorption (b and c) (P = 10 mg/L) on different locations at the surface of the sample.

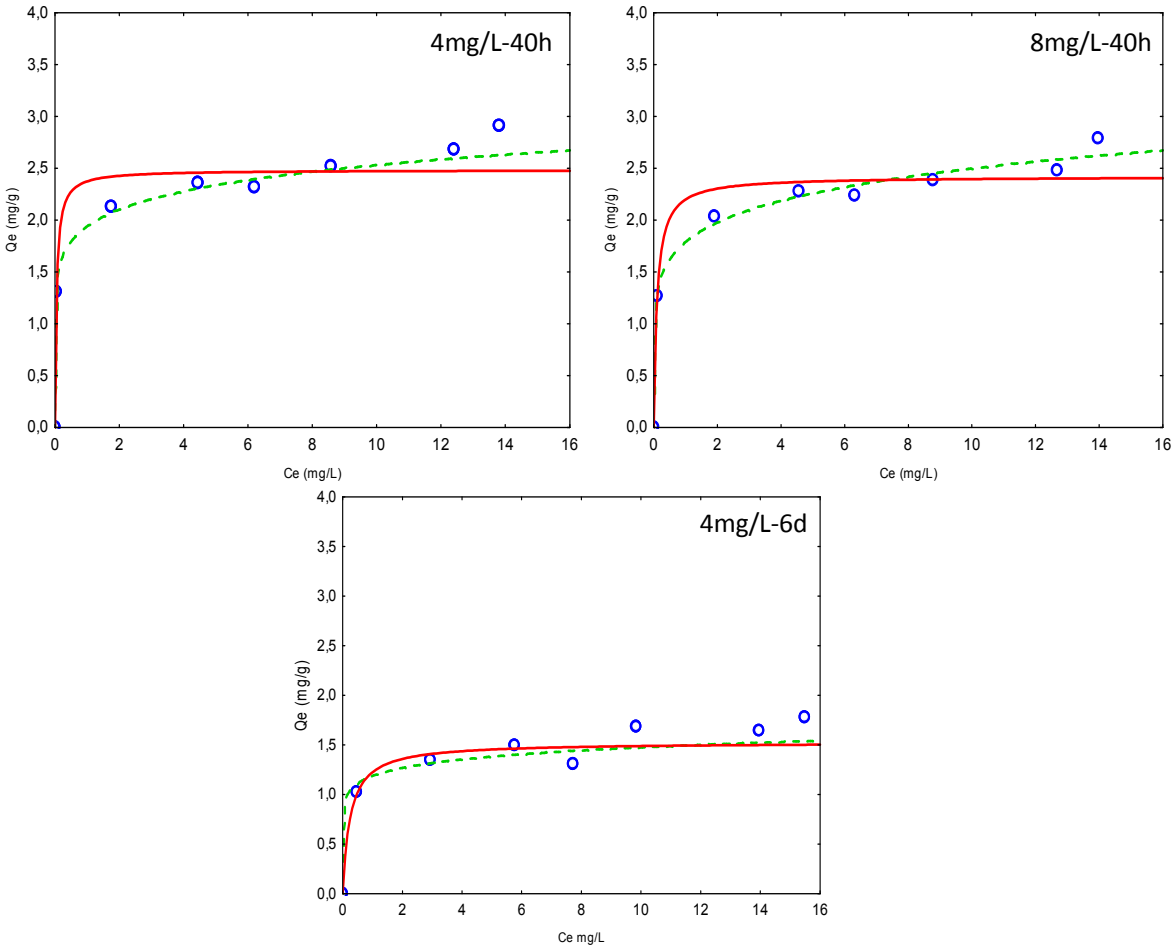

Fig. 6 Adsorption isotherms of phosphate on the different iron byproducts. Experimental data (dots), model fits (curves) Langmuir: full curve, Freundlich: dashed curve. Adsorbent concentration = 1.5 g/L; [P] = 2-20 mg/L, T = 20 °C, NaCl = 0.01 M.

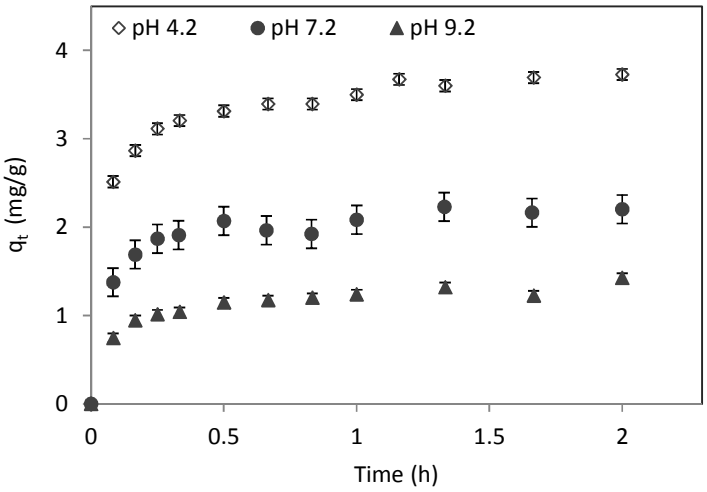

Fig. 7 Adsorption kinetics of phosphate onto iron byproducts. Conditions: [P] = 10 mg/L, adsorbent concentration = 1.5 g/L, pH = 4.2, 7.2 and 9.2, T = 20 °C.